Multiphase density functional theory parameterization of the interatomic potential for silver and gold

Eur. Phys. J. B (2013) 86: 288
DOI: 10.1140/epjb/e2013-40067-6

THE EUROPEAN PHYSICAL JOURNAL B

Regular Article

Multiphase density functional theory parameterization of the interatomic potential for silver and gold

John T. Titantah[1] and Mikko Karttunen[2,a]

[1] Department of Applied Mathematics, The University of Western Ontario, N9A 3K7 London, Ontario, Canada
[2] Department of Chemistry and Waterloo Institute for Nanotechnology, University of Waterloo, N2L 3G1 Waterloo, Ontario, Canada

Received 27 January 2013 / Received in final form 1st May 2013
Published online 24 June 2013 –

Abstract. The ground state energies of Ag and Au in the face-centered cubic (FCC), body-centered cubic (BCC), simple cubic (SC) and the hypothetical diamond-like phase, and dimer were calculated as a function of bond length using density functional theory (DFT). These energies were then used to parameterize the many-body Gupta potential for Ag and Au. We propose a new parameterization scheme that adopts coordination dependence of the parameters using the well-known Tersoff potential as its starting point. This parameterization, over several phases of Ag and Au, was performed to guarantee transferability of the potentials and to make them appropriate for studies of related nanostructures. Depending on the structure, the energetics of the surface atoms play a crucial role in determining the details of the nanostructure. The accuracy of the parameters was tested by performing a 2 ns MD simulation of a cluster of 55 Ag atoms – a well studied cluster of Ag, the most stable structure being the icosahedral one. Within this time scale, the initial FCC lattice was found to transform to the icosahedral structure at room temperature. The new set of parameters for Ag was then used in a temperature dependent atom-by-atom deposition of Ag nanoclusters of up to 1000 atoms. We find a deposition temperature of 500 ± 50 K where low energy clusters are generated, suggesting an optimal annealing temperature of 500 K for Ag cluster synthesis. Surface energies were also calculated via a 3 ns MD simulation.

1 Introduction

Applications of noble metal nanoparticles are currently emerging in medicine where they are used as antimicrobial agents [1], antivirals against HIV-1 [2], antiangiogenic agents [3], in drug delivery [4] and in cancer therapy [4,5]. They are also used in chemical sensory devices due to their enhanced surface chemical activity [6–10]. Ag clusters as small as Ag_7 and Ag_8 supported with mercaptosuccinic acid have been demonstrated to be very potent in water purification through their chemical sensitivity to the presence of heavy metals like Pb, Cd, Hg [11]. The application of noble metal nanoparticles in electronic industry in inkjet printing of conductive lines for circuitory [12] and as electronically conductive adhesives [13–16] results from their electronic properties. Organic memory devices based on DNA biopolymer nanocomposites with Ag nanoparticles have been demonstrated [17]. The large optical forces induced by the transfer of momentum from electromagnetic radiation to a dielectric nanoparticle also make them useful in nano optical manipulation [7,18–20]. It has been shown that subjecting Au nanoparticles to optical forces induces aggregation and enhances the Raman scattering intensity of the thiophenol coverage of the Au nanoparticle [21].

It is common to synthesize noble metal nanoparticle either as free standing or in an inert gas matrix with sizes ranging from one to several hundred nanometers. Ag nanoclusters as small as 4.1 nm and 5.6 nm have been deposited on silicon substrates. Their thermally induced disintegration has been studied, revealing melting at temperatures well below Ag melting temperature [22]. Clusters of few atoms are also routinely isolated by stabilizing them with some protective molecules [22,23]. For example, a 25 atom Au-thiolate cluster in solution [24], dodecanethiol-stabilized-Au_{38} [25], a 1 nm lyzozyme-stabilized-Au nanocluster for Hg^{2+} sensor [26] and DNA-encapsulated 10 atom Ag-cluster [27] have been reported. A small angle X-ray study on the mechanism of Ag nanoparticle formation showed that nanoparticle formation initiates with the formation of Ag_{13} clusters which agglomerate together to form a nanoparticle within 6 ms [28].

The advances in synthesis methods have not been accompanied by an equal increase in understanding of the structural, electronic and optical properties. The nanosized nature gives these particles/clusters properties that are intermediate between molecular – of quantum origin

[a] e-mail: mikko.karttunen@uwaterloo.ca

– and bulk character. Size dependent structural changes have been widely investigated using methods ranging from experiments based on electron diffraction spectroscopy [29,30] to theoretical methods involving classical molecular mechanics approaches [31] and quantum calculations. In particular, pseudopotential time-dependent density functional theory (TDDFT) calculations of the optical absorption of magic number noble metal nanoparticles have been carried out [32]. Crossover from molecular to nanosized behavior was predicted to occur for clusters with around 150 Ag atoms [32]. Calculations of the absorption and the Raman enhancement of Ag_n-pyridine complexes ($n = 2-20$) have been done using TDDFT and both properties were found to depend strongly on the cluster size [33].

Theoretical studies of noble metal clusters are widely based on classical approaches making use of interatomic potentials like the Gupta potential [34,35], the Sutton-Chen potential [36,37] and the embedded atom potential [38,39]. The latter has been used to study the size dependent melting of Ag nanocluster [40], spontaneous alloying in Au-Ag nanoclusters [39] and structural optimization of Ag-Pd [41]. The Gupta potential is widely used in predicting stable structures of noble metal nanoparticles like Ag and Au [42] and bimetallic clusters like Pd-Au [42]. The parameters of the potential are obtained by fitting experimental or DFT [42] data on the bulk face-centered cubic (FCC) system. This does not, however, guarantee transferability of the potential to the different phases of the system. For example, when the resulting potentials are applied to lower coordination states of the material (such as dimers, trimers, etc.), very short bonds and overbinding are obtained rendering the potential inappropriate for studies of low dimensional objects like nanoclusters. This effect has also been demonstrated to explain the finding that the Gupta and Sutton-Chen parameterizations predict different growth patterns already for small Ag clusters [43]. Shao et al. [43] pointed out that due to the flatter nature of the dimer potential as given by the Gupta formulation, it is susceptible to yield more strain-tolerant structures than those generated using the Sutton-Chen potential.

In this study, we use the DFT approach to perform ground state energy calculations on the FCC, BCC, simple cubic, the hypothetical diamond-like phase and dimer. These energy profiles are used to parameterize the Gupta potential. The parameters are given as functions of the coordination number of the Ag and Au atoms-giving them a bond-order character. The appropriateness of the parameters for low coordinated structures is demonstrated.

2 All electron calculation: parameterization of the Gupta potential

We used the WIEN2k all-electron-full-potential linearized-augmented-plane-wave DFT code [44] to calculate the binding energies of Ag and Au in FCC, BCC, simple cubic, diamond-like phases, and dimers. This DFT approach partitions the unit cell into muffin-tin (MT) spheres centred on each atomic site and the interstitial region. Within the MT spheres, the Kohn-Sham functions are given as linear combinations of spherical harmonics weighted by radial functions. In the interstitials they are parameterized as plane-waves. The generalized gradient approximation (GGA) [45] for the exchange and correlation energy is adopted. The two parameters governing the accuracy of the calculation are the number of plane-waves in the Brillouin zone and the plane-wave vector **k** cut-off parameter-RKM. This latter parameter is the product of the maximum plane wave vector in the interstitial region and the smallest muffin-tin radius in the system. For the calculations, the total number of **k**-points used to describe the Kohn-Sham orbitals in the interstitials ranged from 1000 to 3000, depending on the lattice type. This, with the RKM value of 6, was found to converge the binding energies to an accuracy of 3 mRy per atom.

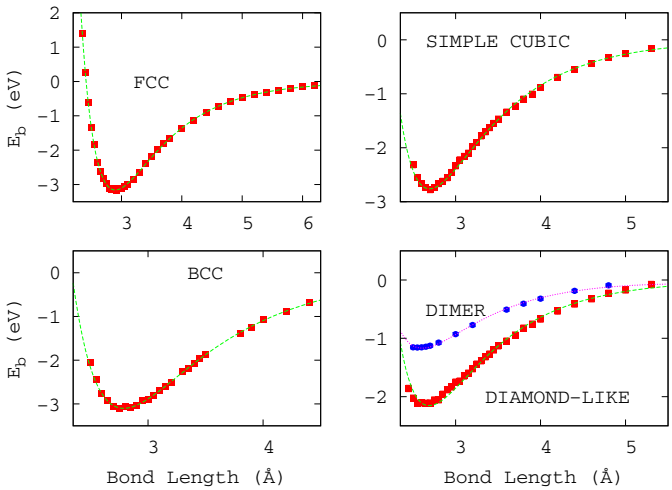

Fig. 1. Energy per Ag atom as a function of distance between atoms for five phases of Ag: FCC, BCC, simple cubic, the diamond-like phase and dimer.

Non-magnetic calculations were performed since both bulk Ag and Au are known to be non-magnetic. For each of the noble metal structures, energy-bond length dependencies were obtained. From them, extrapolation to very large lattice parameters permitted the isolated atom values to be removed yielding the binding energies as shown in Figures 1 and 2. For FCC Ag, we find an equilibrium lattice parameter of 4.07 ± 0.02 Å and a binding energy of 3.16 ± 0.04 eV/atom. The former compares very well with the measured value of 4.09 Å while the binding energy overestimates the measured value of 2.95 eV [46] by about 7%. The bulk modulus was found to be 106 ± 2 GPa which is in excellent agreement with the experimental value of 109 GPa at 0 K [47]. For Au, a lattice parameter of 4.09 ± 0.02 Å (see Fig. 3a) compares very well with the measured value of 4.08 Å. The binding energy of 4.01 ± 0.04 eV, however, overestimates the experimental value of 3.81 eV [46,48,49]. The bulk modulus of 179 ± 2 GPa is in excellent agreement with experimentally measured value of 180 GPa at 0 K [47].

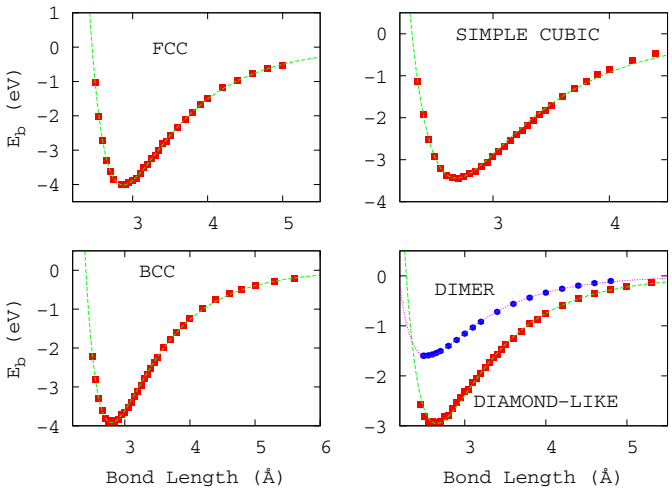

Fig. 2. Energy per Au atom as a function of distance between atoms for five phases of Au: FCC, BCC, simple cubic, the diamond-like phase and Au dimer.

The BCC phase is less stable than the FCC phase by about 0.06 (0.08) eV/atom for Ag (Au) and is, thus, predicted to be the high pressure phase of these materials. This is in agreement with another theoretical work that predicted the same result for Au [50]. The small energy difference between the BCC and the FCC phases of Ag is a possible reason for the recently observed continuous and reversible BCC-FCC phase transformation in Ag/V multilayers [51].

We used these energy-lattice parameter (or energy-bond length $E-r$) dependencies to parameterize the Gupta potential for Ag and Au. For this, we rescaled the binding energies by a factor of 0.934 (0.951) for Ag (Au) to equate the FCC value with the experimentally measured value while rescaling distances by a factor of 1.006 (0.996) for Ag (Au) to equate to the corresponding FCC experimental bond length of 2.889 Å (2.884 Å). The bulk moduli become 99 GPa for Ag and 170 GPa for Au. Most of the parameterizations that have been done are based on the bulk properties of these materials which are in the FCC phase [42,43]. To our knowledge, this is the first attempt to develop parameters that make the potential transferable enough for use in various phases. These new parameters should therefore be appropriate in high temperature studies of these metals and for low-dimensional structures formed from them.

For this potential, the energy of atom i is given by [52]:

$$V_i = V_i^r - V_i^a, \tag{1}$$

where the repulsive part of the potential is given by:

$$V_i^r = \frac{1}{2}\sum_{j\neq i} \alpha \exp\left[-\lambda\left(\frac{r_{ij}}{R_0}-1\right)\right] \tag{2}$$

and the attractive part by:

$$V_i^a = \frac{1}{2}\left[\sum_{j\neq i} \beta^2 \exp\left[-2\mu\left(\frac{r_{ij}}{R_0}-1\right)\right]\right]^{1/2}. \tag{3}$$

In the first approximation, the phase dependence of this potential is introduced by adopting a coordination dependence of the parameters: coordination is defined by introducing a cut-off function f_c as in the Tersoff potential [53]

$$f_c(x) = \begin{cases} 1 & ; x \le R_c - D \\ \frac{1}{2}\left[1-\sin\left(\frac{\pi}{2}\frac{x-R_c}{D}\right)\right] & ; |x-R_c| < D \\ 0 & ; x \ge R_c + D \end{cases} \tag{4}$$

by which coordination n_{ci} is given by:

$$n_{ci} = \sum_{j\in \mathrm{Nei}(i)} f_c(r_{ij}), \tag{5}$$

where $\mathrm{Nei}(i)$ is the set of nearest neighbor atoms of atom i. A continuous and differentiable cut-off function is chosen for the convenience of force calculations. We set $R_c = 3.1$ Å and $D = 0.1$ Å. The parameters λ and μ are obtained from the FCC potential (Figs. 1 and 2) as previous values for Ag [43] and Au [42] did not permit a good fit of our DFT calculations. The Tersoff potential has been used in a similar manner to construct a water [54] model which reproduces many of the important thermodynamical anomalies of water.

The parameters $\alpha(n_c)$, $\beta(n_c)$ and $R_0(n_c)$ in equations (2) and (3) are given as functions of the coordination number of the atoms (and, therefore, of the phases). On a more practical note, when this potential is used on systems in which neighbouring atoms have differing coordination structure like surfaces and interfaces, these parameters are obtained for such pairs of atoms i and j by taking the average coordination number around these interacting atoms.

We suggest here the following simple functional forms:

$$\begin{aligned} \alpha(n_c) &= \alpha_\infty\left(1+\zeta Ł\left(\frac{n_c+n_0}{\delta}\right)\right) \\ \beta(n_c) &= \beta_\infty\left(1+\gamma Ł\left(\frac{n_c+\Delta}{\eta}\right)\right) \\ R_0(n_c) &= R_\infty\left[1-\frac{\rho_0}{(1+(n_c/\nu)^\xi)}\right], \end{aligned} \tag{6}$$

where $Ł(x) = 2\left(\exp\left(-x^2\right)-1+x^2\right)/x^4$.

Fits to these functional forms are performed as shown in Figures 3 and 4 for Ag and Au, respectively. In the fitting procedure, periodic images are included such that interactions between atoms separated by distances as far as 9 Å are included. The parameters are listed in Table 1.

The effect of this new parameterization for Ag and Au clusters is that in lower coordination environments (such as surfaces), the atoms become less energetic. For example, the energy per atom of an Ag dimer was found to be 1.09 eV. This compares better with the experimental value of 0.83 ± 0.02 eV [55] than the previously obtained values of 1.22 eV [43] and 1.40 eV [41,56]. Also the dimer bond length of 2.59 Å is in good agreement

Table 1. Parameters of the Gupta potential for Ag and Au.

	λ	μ	α_∞ (eV)	ζ	n_0	δ	β_∞(eV)	γ	Δ	η	R_∞(Å)	ρ_0	ν	ξ
Ag	10.167	3.105	0.1613	6.939	–0.616	1.848	2.1585	0.592	–0.901	3.470	3.053	0.172	8.710	2.452
Au	12.728	3.173	0.1730	6.5149	–1.234	1.593	2.7565	0.628	–2.041	1.952	2.927	0.144	6.247	3.330

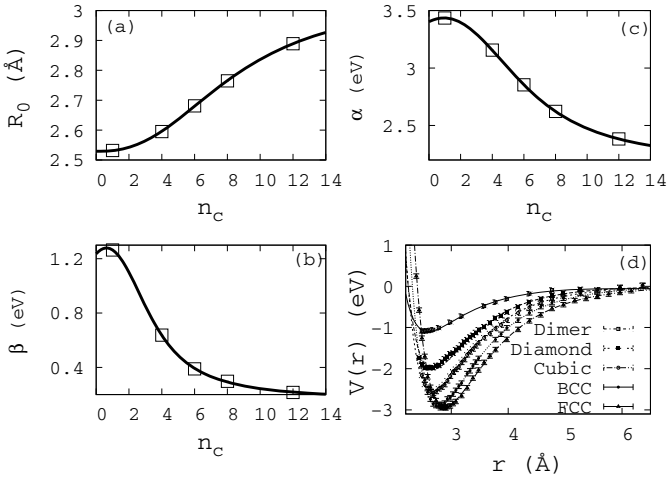

Fig. 3. DFT parameters of the Gupta potential for the four phases of Ag: FCC, BCC, simple cubic, diamond-like phase and dimer. The fitted potentials are shown in panel (d) and the points are the corresponding DFT binding energies.

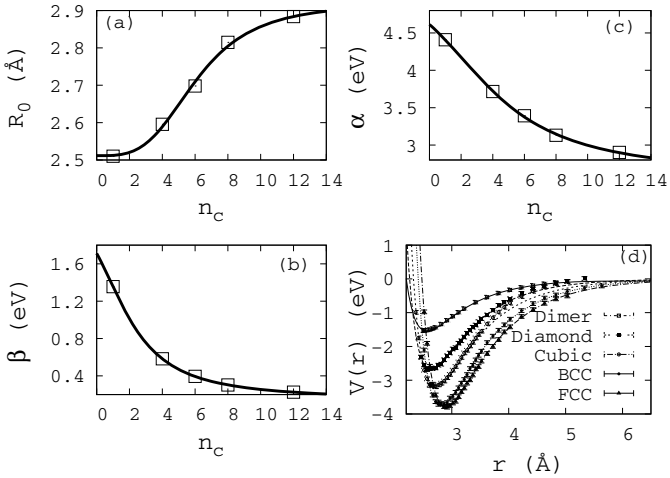

Fig. 4. DFT-parameters of the Gupta potential for the five phases of Au: face-centered cubic, BCC, simple cubic, Au in the diamond-like phase and dimer. The fitted potentials are shown in panel (d) and the points are the corresponding DFT binding energies.

with the measured value of 2.53 Å [55,57,58] as compared to values of 2.37 Å [43] and 2.43 Å [41,56] that result from the previous parameterizations. The best DFT dimer energy so far is 0.9 eV with a corresponding dimer bond length of 2.58 Å [59]. The Au dimer bond length of 2.56 Å compares very well with the experimental value of 2.47 Å [60] whereas previous parameterization sets this value at 2.3 Å [42]. Also, the dissociation energy per atom of 1.53 eV for Au_2 is much closer to the experimental value of 1.15 eV [61] than the value of 2.42 eV that previous parameterization gives [42]. The observations made here about the properties of dimers are also valid for other low coordinations such as 2-, 3- and 4-coordinated atoms.

The implication of the weaker binding of lower coordinated atoms – as opposed to the strong binding obtained with the previous parameters [41–43] – in studies of Ag and Au nanoclusters is that surface atoms will become more mobile. This results in the nanoclusters experiencing surface premelting at lower temperatures. Thus, the current parameterizations may be very appropriate in surface studies.

To demonstrate that the strain-tolerant nature of previous Gupta parameters [41–43] for Ag and Au has been improved, we plot the second derivative of the dimer potential in Figure 5. Our results show higher curvature at all dimer separations demonstrating that the current parameterization will not accommodate strained systems.

A series of constant temperature MD was performed to check the performance of the potential and the new parameters in characterizing the properties of Ag clusters and surfaces. Temperature was kept constant by using the

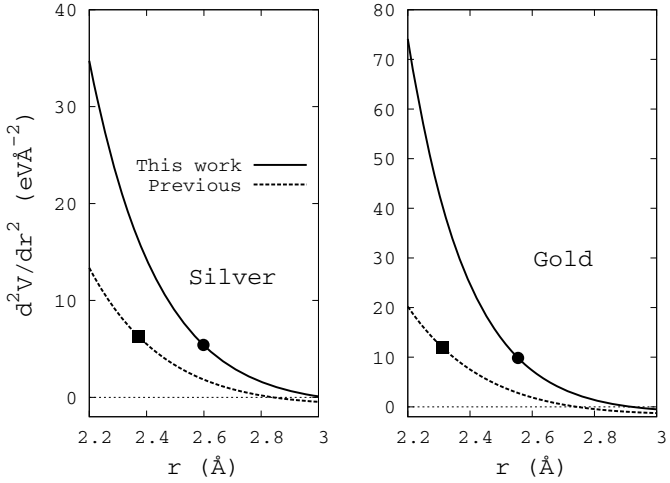

Fig. 5. The second derivative of the Ag_2 and Au_2 dimer potentials. Our results are shown as full lines while previous parameterizations [41–43] are shown as dashed lines. The points locate the curvature at the corresponding equilibrium distances.

Nosé-Hoover thermostat [62,63] and the velocity-Verlet algorithm was used.

We evaluated the vacancy energy by performing pairs of 600 ps MD simulations: one for a 864 atom periodic cell and another with a vacancy created in the same 864 atom system. Simulations were performed at 300 K and 600 K and the energy of the vacancy was calculated from both

calculations by averaging over 500 ps as:

$$e_v = (N-1)\left[e(N-1) - e(N)\right], \tag{7}$$

where $e(N)$ is the energy per atom of an N-atom system. Using the previous parameters for Ag [43], we found a vacancy energy of 0.88 ± 0.02 eV for both temperatures. Our parameters give values of 0.94 ± 0.03 eV and 0.98 ± 0.03 eV at 300 and 600 K, respectively. These latter results compare very well with measurements that situate the silver vacancy energy between 0.99 and 1.16 eV [64].

Surface energies γ were calculated by performing 3 ns MD simulations of Ag clusters of diameter 3.4 nm made of $N = 935$ atoms. The surface energy was calculated as:

$$e_s = \frac{N\left[e(N) - e_{\text{bulk}}\right]}{4\pi R^2}, \tag{8}$$

where e_{bulk} is the bulk energy per atom, $e(N)$ the energy per atom of an N-atom silver cluster and R is the radius of the cluster. We obtained a surface energy of $0.88\,\text{J/m}^2$ using our parameterization. Using the previous parameterization [43] gave $0.70\,\text{J/m}^2$. Our result is closer to ab initio value of $1.08\,\text{J/m}^2$ obtained on a 249 atom cluster [65].

The surface energy γ of the (100), (110) and (111)-oriented surfaces of Ag were also calculated on slabs which were appropriately oriented and periodically repeated in the lateral directions. The surface energies were calculated from 1 ns MD runs using equation (8) with the $4\pi R^2$ denominator replaced by twice the surface area of one of the face of the slabs. The surface energies were calculated at different temperatures using the current and previous parameters. The results in Figure 6, obtained as statistical averages over 600 ps, show that the order of the surface energy per atom of (100) < (111) < (110) is maintained by the present and earlier parameterizations [43]. However, the previous parameters underestimate γ as compared to experimental surface energy of 0.57 eV/atom ($1.25\,\text{J/m}^2$) [66,67] and ab initio results [67–69]. Our zero-temperature surface energy of about 0.5 eV/atom ($1.1\,\text{J/m}^2$) for the (111)-surface is in excellent agreement with DFT values of 0.49 eV/atom [67] and 0.5 eV/atom [70], and the experimental value of 0.57 eV/atom [66]. The value 0.40 eV/atom for the (100)-surface is very close to the ab initio value of 0.41 eV/atom [71], although the (111) value of 0.32 eV/atom obtained by the latter authors is very low compared to ours and measurements [66]. The use of Sutton-Chen potential gives values of 0.52 eV/atom ($0.99\,\text{J/m}^2$), 0.78 eV/atom ($1.06\,\text{J/m}^2$) and 0.42 eV/atom ($0.92\,\text{J/m}^2$) for the (100), (110) and (111)-surfaces, respectively [72]. Using the embedded-atom functions, Foiles et al. [69] obtained values of 0.37 eV/atom ($0.71\,\text{J/m}^2$), 0.57 eV/atom ($0.77\,\text{J/m}^2$) and 0.28 eV/atom ($0.62\,\text{J/m}^2$), for the (100), (110) and (111)-surfaces, respectively. They are considerably lower than experimental surface energy of Ag. The current parameters, therefore, improve the surface energies by more than 20% as compared to widely used classical potentials.

Kohn-Sham DFT calculations on small (2−12 atoms) Ag clusters has demonstrated an even-odd oscillation in the stability of silver clusters which is attributed to spin subshell closing [73]. Although the current level of parameterization does not include spin effects (unlike DFT [73]), but we performed a dynamic search for the global energy minima of small silver clusters using our parameterization and a previous one [43]. Apart from Ag_3 for which the current and previous parameterizations find the equilateral triangular shape the most stable structure, both parameter sets fail to reproduce the planar structures of Ag_4, Ag_5 and Ag_6 as the most stable ones, but rather suggest them to adopt two isomeric structure: planar and 3D structures with an almost vanishing energy difference between them. For example, with our parameterization we find the 3D prism structure for Ag_4 to be lower in energy by 2 meV as compared to the 2D rhombus. The parameters of Shao et al. [43] find the prism to be lower by 8 meV. The failure in predicting the 2D structures of small clusters (Ag_n, $n = 4, 5, 6$) as the most stable ones may be related to the missing angular dependence which should account for hybridization of the p-orbitals of small silver clusters. For higher index clusters (Ag_7 and above), however, the 3D structures are found to be the most stable.

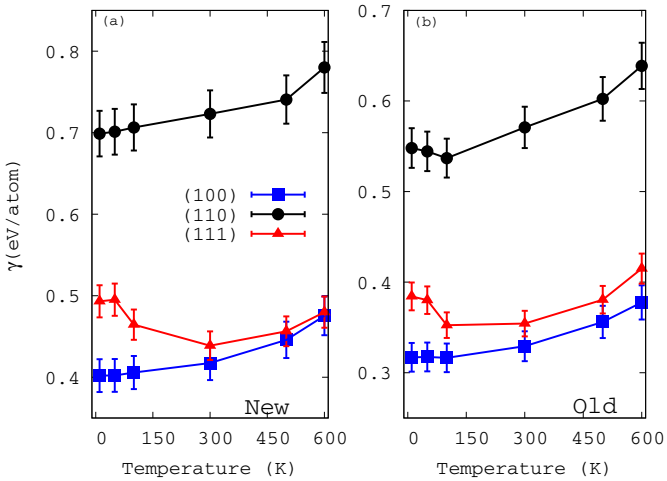

Fig. 6. The surface energy per atom for current and previous parameters for (100)-(rectangle), (110)-(circle) and (111)-(triangle) oriented silver surfaces at low temperature. The results of the current work are on the left panel (a) and those of previous [43] are in panel (b).

3 Relaxation of Ag_{55} cluster and MD deposition of Ag clusters

We performed a 2 ns MD simulation to relax a 55 atom Ag cluster at 300 K. The cluster's structure was transformed from a 4-shell cluster to a 3-shell within the first 10 ps. Figure 7 shows the density distribution as a function of distance from the central atom. The cluster is characterized by a central atom, a Ag_{12} first-shell of radius 2.74 Å, a next shell of 30 Ag atoms of radius 4.73 Å and an outermost shell of 12 atoms of radius 5.45 Å. The final structure of the cluster is shown in the right of Figure 7.

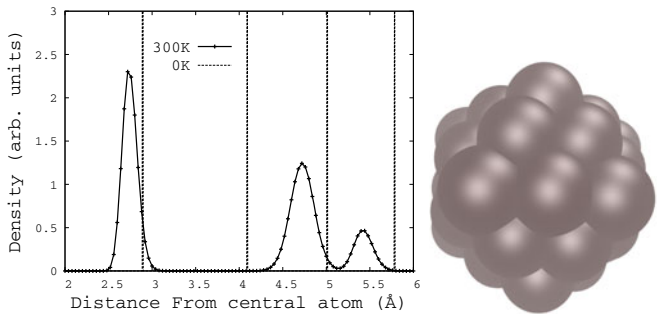

Fig. 7. Left: density distribution as a function of distance from the central atom of a Ag_{55} cluster for the unrelaxed (thin-dotted line) and the MD-relaxed structure at 300 K (full line). The feature at 4.09 Å in the unrelaxed cluster shifts upwards and merges with the feature at 5.0 Å which shifts downwards. Right: snapshot of MD-relaxed cluster at the end of the 2 ns simulation.

To further test our parameters, we performed an atom by atom molecular dynamic deposition of Ag nanoclusters of up to 1000 atoms. The starting configuration was a Ag_4 cluster with four Ag atoms sitting at the corners of a square. While the cluster is undergoing relaxation at a fixed temperature, an atom is initiated far away (4 nm from the center of the formed cluster) with a kinetic energy of 2 eV and velocity pointing toward the cluster center, with the position of the atom chosen randomly on the sphere of radius 4 nm. Once this atom has entered the field of the relaxing cluster (distance less than 3.5 Å from the closest cluster atom) its dynamics are included in the Nosé-Hoover thermostating scheme. The resulting cluster is relaxed for 100 ps and the process is repeated for subsequent atoms. Similar deposition process was done using the old parameters [43].

Figure 8 shows the evolution of the energy per atom as the cluster size grows at different temperatures using both the new and old sets of parameters. We find that the energy decreases monotonically as the cluster size increases at all temperatures except at temperature 500 ± 50 K, where sudden drops in energy were recorded for cluster sizes larger than 126 and 150 for the old parameters, and 150 and 192 for the new set of parameters. We fitted the energy per atom as a function of the cluster size with the function [74]

$$e(T) = \frac{E(N,T)}{N} = e_\infty(T) + bN^{-1/3} + cN^{-2/3} + dN^{-1}, \quad (9)$$

where $E(N,T)$ is the total energy of an N-atom Ag cluster at temperature T (in Kelvin). The temperature dependence of the extrapolated large cluster energy, e_∞, is shown in the inset and reveals lower energy clusters at a temperature of 500 ± 50 K. Note the big drop in energy as the temperature is raised from 300 K to 500 K for the new parameters and the almost constant value of the energy when the old parameters are used. This indicates that the current set of parameters predicts an optimal temperature of 500 K at which there is a kinetically-driven structural or morphological transformation of small and medium-size

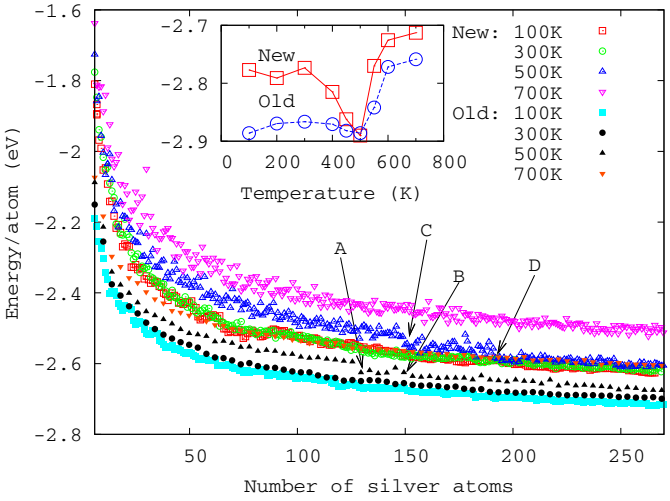

Fig. 8. The evolution of the energy per atom vs. Ag cluster size at different deposition temperatures. Open symbols: new parameters, closed symbols: old [43]. The arrows indicate points of energy drops. Inset: temperature dependence of e_∞ (see Eq. (9)).

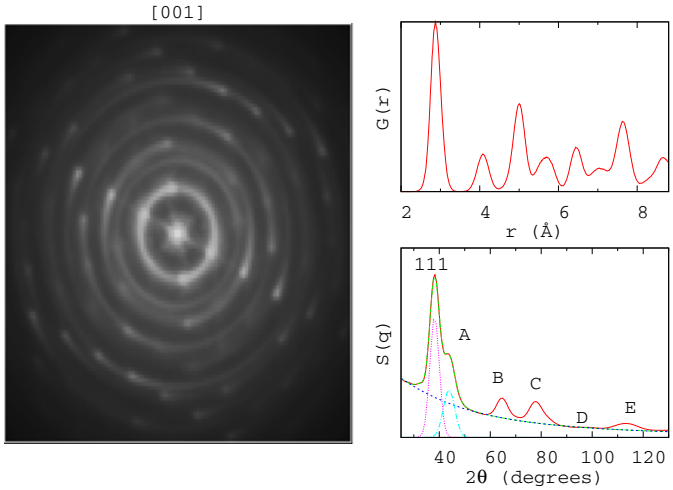

Fig. 9. The lattice structure of a 561 atom Ag nanocluster generated by MD deposition at 500 K and annealed at 300 K. The electron diffraction pattern (left) is calculated by using the Hartree-Fock parameterized form factors of Doyle and Turner [75]. The density distribution with respect to the central atom, $G(r)$, (top-right) shows a highly ordered crystal and the structure factor $S(q)$ (lower-right) shows well defined features. The (111) spot can clearly be seen. Other spots (200), (220), (311)/(222), (400) and (331)/(420) are clearly visible and denoted as A, B, C, D and E, respectively. The lines in the lower-right panel are for the functions used to fit the (111) spot.

Ag clusters into more energetically favourable ones. It also shows that it may be capable of distinguishing between the various temperature induced structural changes within Ag nanoclusters.

Typical structural properties of a 561 atom Ag cluster atom-by-atom deposited at 500 K and annealed at 300 K with the new set of parameters is shown in Figure 9.

We calculated the electron diffraction pattern by using the Hartree-Fock atomic form factors as parameterized by Doyle and Turner [75]. The atomic distribution with respect to the central atom of the cluster $G(r)$, shows a highly ordered nanocluster, with FCC order up to a radius of more than 1 nm . This is also confirmed by the structure factor $S(q)$, with $q = \frac{\sin\theta}{\lambda}$, λ being the wave length and θ is the Bragg's diffraction angle. All results are averages over 10 ns in time intervals of 200 fs. The assignment of the spots agree excellently with that of Khan et al. [76] on Ag nanoparticles and Kang et al. [77] on sintered inkjet-printed Ag nanoparticles. In particular, the electron diffraction pattern is quite similar to the high resolution transmission electron microscopy (HRTEM) measurement of reference [76] on Ag nanoparticles of size 16.37 nm . $G(r)$ also shows that the 561 atoms cluster has a diameter of about 2.5 nm , which is also confirmed by size L of 24.97 ± 0.21 Å, obtained based on the position $2\theta = 38.16°$ and the full-width at half-maximum (FWHM) $\sigma = 4.24°$ of the (111) spot as [76,78,79]

$$L = \frac{0.94\lambda}{\sigma \cos 2\theta}, \tag{10}$$

where σ is in radians and the wavelength $\lambda = 0.1541$ nm is used. The 2θ and σ values are obtained from a fit (in the interval $\pm 12°$ around the (111) spot) with a sum of three Gaussians and a Lorentzian, with the latter centered at $q = 0$. A similar calculation on a 2093 atoms cluster cut out of bulk Ag and relaxed at 300 K yielded a diameter of 4.22 ± 0.29 nm which was also quite close to its size of 4.2 nm obtained on the basis of $G(r)$.

4 Conclusion

We performed DFT calculations of the binding energies of Ag and Au in five different phases: FCC, BCC, simple cubic, diamond-like and dimer. We computed the corresponding equilibrium bond lengths, binding energies and bulk moduli, and found them to compare very well with experimentally reported values. We used the binding energy versus bond length dependencies to perform a cross-phase parameterization of the many-body Gupta potential for Ag and Au. The new parameters, whose coordination-number dependencies are fitted to simple analytical functions, are done so as to correctly describe the energetic and structural behavior of low coordinated noble metal atoms sitting in dimer, linear chains, diamond-like environment, etc. We believe that these new parameterizations should be appropriate for studies of low dimensional structures such as nanoclusters and surfaces. In order to demonstrate the improved accuracy of this potential, we have shown that the surface energies of the most common Ag surfaces obtained using this potential compare better with experimental and ab initio than previous parameterizations. They may also be used to reconcile the structural differences reported for medium-sized clusters of noble metals generated using the traditional bulk-fcc-based parameters of the Gupta potential – which is susceptible to yield more strained structures – and the Sutton-Chen potential, which leads to less-strained structures [43]. The current parameterization of the Gupta potential solves the problem of strain-torlerance reported for the parameters of Shao et al. [43] as the broadness at the bottom of the dimer potential well is improved. The current parameterization only considers local atomic coordination. It does not account for angular degrees of freedom. The lack of this in the current and previous potentials is one of the major reasons for their inability to predict the 3-dimensional structure of Ag_n $(n = 4, 5, 6)$. Incorporating this will be the subject of our subsequent studies.

We would like to thank Martin Müser and Jari Jalkanen for critical reading of the manuscript. This work was supported by the Natural Sciences and Engineering Research Council of Canada (MK). Computational resources were provided by SharcNet [www.sharcnet.ca].

References

1. J.S. Kim et al., Nanomed. Nanotechnol. Biol. Med. **3**, 95 (2007)
2. H.H. Lara, L. Ixtepan-Turrent, E.N. Garza Trevino, D.K. Singh, J. Nanobiotechnology **9**, 38 (2011)
3. S. Gurunathan, K.J. Lee, K. Kalishwaralal, S. Sheikpranbabu, R. Vaidyanathan, S.H. Eom, Biomat. **30**, 6341 (2009)
4. N. Portney, M. Ozkan, Anal. Bioanal. Chem. **384**, 620 (2006)
5. X. Huang, I. El-Sayed, W. Qian, M. El-Sayed, J. Am. Chem. Soc. **128**, 2115 (2006)
6. Y.Q. Chen, C.J. Lu, Sens. Actuators B Chem. **135**, 492 (2009)
7. E. Filippo, A. Serra, D. Manno, Sens. Actuators B Chem. **138**, 625 (2009)
8. X. He, C. Hu, H. Liu, G. Du, Y. Xi, Y. Jiang, Sens. Actuators B Chem. **144**, 289 (2010)
9. M.R.H. Nezhad, J. Tashkhourian, J. Khodaveisi, J. Iran. Chem. Soc. **7**, S83 (2010)
10. R.F. Ngece, N. West, P.M. Ndangili, R.A. Olowu, A. Williams, N. Hendricks, S. Mailu, P. Baker, E. Iwuoha, Int. J. Electrochem. Sci. **6**, 1820 (2011)
11. M.S. Bootharaju, T. Pradeep, Langmuir **27**, 8134 (2011)
12. H. Lee, K. Chou, K. Huang, Nanotechnology **16**, 2436 (2005)
13. D. Chen, X. Qiao, X. Qiu, J. Chen, J. Mater. Sci. **44**, 1076 (2009)
14. S.L.C. Hsu, R.T. Wu, Mater. Lett. **61**, 3719 (2007)
15. H. Lee, K. Chou, Z. Shih, Int. J. Adhes. Adhes. **25**, 437 (2005)
16. A. Hu, J.Y. Guo, H. Alarifi, G. Patane, Y. Zhou, G. Compagnini, C.X. Xu, Appl. Phys. Lett. **97**, 153117 (2010)
17. Y.C. Hung, W.T. Hsu, T.Y. Lin, L. Fruk, Appl. Phys. Lett. **99**, 253301 (2011)
18. A. Ashkin, Phys. Rev. Lett. **24**, 156 (1970)
19. A. Ashkin, J.M. Dziedzic, J.E. Bjorkholm, S. Chu, Opt. Lett. **11**, 288 (1986)

20. M. Liu, T. Zentgraf, Y. Liu, G. Bartal, X. Zhang, Nat. Nanotechnol. **5**, 570 (2010)
21. F. Svedberg, M. Kall, Faraday Disc. **132**, 35 (2006)
22. S.R. Bhattacharyya, D. Datta, I. Shyjumon, B.M. Smirnov, T.K. Chini, D. Ghose, R. Hippler, J. Phys. D **42**, 035306 (2009)
23. C.A.J. Lin, C.H. Lee, J.T. Hsieh, H.H. Wang, J.K. Li, J.L. Shen, W.H. Chan, H.I. Yeh, W.H. Chang, J. Med. Biol. Eng. **29**, 276 (2009)
24. M.A. MacDonald, D.M. Chevrier, P. Zhang, H. Qian, R. Jin, J. Phys. Chem. C **115**, 15282 (2011)
25. H. Qian, M. Zhu, U.N. Andersen, R. Jin, J. Phys. Chem. A **113**, 4281 (2009)
26. H. Wei, Z. Wang, L. Yang, S. Tian, C. Hou, Y. Lu, Analyst **135**, 1406 (2010)
27. J.T. Petty, C. Fan, S.P. Story, B. Sengupta, A.S.J. Iyer, Z. Prudowsky, R.M. Dickson, J. Phys. Chem. Lett. **1**, 2524 (2010)
28. M. Takesue, T. Tomura, M. Yamada, K. Hata, S. Kuwamoto, T. Yonezawa, J. Am. Chem. Soc. **133**, 14164 (2011)
29. D. Reinhard, B. Hall, D. Ugarte, R. Monot, Phys. Rev. B **55**, 7868 (1997)
30. M. Blom, D. Schooss, J. Stairs, M. Kappes, J. Chem. Phys. **124**, 244308 (2006)
31. X. Yang, W. Cai, X. Shao, J. Phys. Chem. A **111**, 5048 (2007)
32. H.C. Weissker, C. Mottet, Phys. Rev. B **84**, 165443 (2011)
33. L. Jensen, L.L. Zhao, G.C. Schatz, J. Phys. Chem. C **111**, 4756 (2007)
34. F. Cleri, V. Rosato, Phys. Rev. B **48**, 22 (1993)
35. K. Michaelian, N. Rendon, I. Garzon, Phys. Rev. B **60**, 2000 (1999)
36. A.P. Sutton, J. Chen, Philos. Mag. Lett. **61**, 139 (1990)
37. J. Doye, D. Wales, New J. Chem. **22**, 733 (1998)
38. J. Mei, J.W. Davenport, G.W. Fernando, Phys. Rev. B **43**, 4653 (1991)
39. T. Shibata, B.A. Bunker, Z.Y. Zhang, D. Meisel, C.F. Vardeman, J.D. Gezelter, J. Am. Chem. Soc. **124**, 11989 (2002)
40. S. Zhao, S. Wang, H. Ye, J. Phys. Soc. Jpn **70**, 2953 (2001)
41. X. Wu, Y. Wu, X. Kai, G. Wu, Y. Chen, Chem. Phys. **390**, 36 (2011)
42. F. Pittaway, L.O. Paz-Borbon, R.L. Johnston, H. Arslan, R. Ferrando, C. Mottet, G. Barcaro, A. Fortunelli, J. Phys. Chem. C **113**, 9141 (2009)
43. X. Shao, X. Liu, W. Cai, J. Chem. Theor. Comput. **1**, 762 (2005)
44. P. Blaha, K. Schwarz, P. Sorantin, S.B. Trickey, Comput. Phys. Commun. **59**, 399 (1990)
45. J.P. Perdew, K. Burke, M. Ernzerhof, Phys. Rev. Lett. **77**, 3865 (1996)
46. C. Kittel, *Introduction to Solid State Physics*, 4th edn. (John Wiley & Sons, Inc., New York, 1971)
47. J. Neighbours, G. Alers, Phys. Rev. **111**, 707 (1958)
48. R.L. Chantry, W. Siriwatcharapiboon, S.L. Horswell, A.J. Logsdail, R.L. Johnston, Z.Y. Li, J. Phys. Chem. C **116**, 10312 (2012)
49. M. Needels, A.M. Rappe, P.D. Bristowe, J.D. Joannopoulos, Phys. Rev. B **46**, 9768 (1992)
50. P. Soderlind, Phys. Rev. B **66**, 176201 (2002)
51. Q.M. Wei, X.Y. Liu, A. Misra, Appl. Phys. Lett. **98**, 111907 (2011)
52. F. Cleri, V. Rosato, Phys. Rev. B **48**, 22 (1993)
53. J. Tersoff, Phys. Rev. B **37**, 6991 (1988)
54. C.L. Dias, T. Ala-Nissila, M. Grant, M. Karttunen, J. Chem. Phys. **131**, 054505 (2009)
55. M. Morse, Chem. Rev. **86**, 1049 (1986)
56. F.R. Negreiros, Z. Kuntova, G. Barcaro, G. Rossi, R. Ferrando, A. Fortunelli, J. Chem. Phys. **132**, 234703 (2010)
57. V. Beutel, H.G. Kramer, G.L. Bhale, M. Kuhn, K. Weyers, W. Demtroder, J. Chem. Phys. **98**, 2699 (1993)
58. G. Wang, J. BelBruno, S. Kenny, R. Smith, Phys. Rev. B **69**, 195412 (2004)
59. S. Nigam, C. Majumder, Langmuir **26**, 18776 (2010)
60. K. Huber, H. Hertzberg, *Molecular Spectra and Molecular Structure Constants of Diatomic Molecules* (van Nostrand, New York, 1979), Vol. 4
61. A. James, P. Kowalczyk, B. Simard, J. Pinegar, M. Morse, J. Mol. Spectrosc. **168**, 248 (1994)
62. S. Nosé, Mol. Phys. **52**, 255 (1984)
63. W.G. Hoover, Phys. Rev. A **31**, 1695 (1985)
64. W. Triftshauser, J.D. McGervey, Appl. Phys. **6**, 177 (1975)
65. I. Vasiliev, B. Medasani, Surface properties of silver and aluminum nanoclusters - art. no. 690207, in *Quantum dots, particles, and nanoclusters V*, edited by K. Eyink, F. Szmulowicz, D. Huffaker (SPIE, 2008). ISBN 978-0-8194-7077-5/ Conference on Quantum Dots, Particles, and Nanoclusters IV, San Jose, CA (2008)
66. W.R. Tyson, W.A. Miller, Surf. Sci. **62**, 267 (1977)
67. L. Vitos, A.V. Ruban, H.L. Skriver, J. Kollar, Surf. Sci. **411**, 186 (1998)
68. V. Fiorentini, M. Methfessel, J. Phys.: Condens. Matter **8**, 6525 (1996)
69. S.M. Foiles, M.I. Baskes, M.S. Daw, Phys. Rev. B **33**, 7983 (1986)
70. H.L. Skriver, N.M. Rosengaad, Phys. Rev. B **46**, 7157 (1992)
71. W. Zhang, Y. Liu, R. Cao, Z. Li, Y. Zhang, Y. Tang, K. Fan, J. Am. Chem. Soc. **130**, 15581 (2008)
72. B.D. Todd, R.M. Lynden-Bell, Surf. Sci. **281**, 191 (1993)
73. R. Fournier, J. Chem. Phys. **115**, 2165 (2001)
74. W. Huang, X. Lai, R. Xu, Chem. Phys. Lett. **507**, 199 (2011)
75. P.A. Doyle, P.S. Turner, Acta Cryst. A **24**, 390 (1968)
76. M.A.M. Khan, S. Kumar, M. Ahamed, S.A. Alrokayan, M.S. AlSalhi, Nano. Res. Lett. **6**, 434 (2011)
77. J.S. Kang, J. Ryu, H.S. Kim, H.T. Hahn, J. Electron. Mater. **40**, 2268 (2011)
78. H.P. Klug, L.E. Alexander, *X-ray diffraction procedures for polycrystaline and amorphous material* (Wiley, New York, 1954)
79. R. Govindaraj, R. Kesavamoorthy, R. Mythili, B. Viswanathan, J. Appl. Phys. **90**, 958 (2001)